Multiple spectral-spatial classification approach for hyperspectral data

Yuliya Tarabalka, Jon Atli Benediktsson, Jocelyn Chanussot, James Tilton

Multiple Spectral–Spatial Classification Approach for Hyperspectral Data

Yuliya Tarabalka, *Student Member, IEEE*, Jón Atli Benediktsson, *Fellow, IEEE*, Jocelyn Chanussot, *Senior Member, IEEE*, and James C. Tilton, *Senior Member, IEEE*

***Abstract*—A new multiple-classifier approach for spectral–spatial classification of hyperspectral images is proposed. Several classifiers are used independently to classify an image. For every pixel, if all the classifiers have assigned this pixel to the same class, the pixel is kept as a marker, i.e., a seed of the spatial region with a corresponding class label. We propose to use spectral–spatial classifiers at the preliminary step of the marker-selection procedure, each of them combining the results of a pixelwise classification and a segmentation map. Different segmentation methods based on dissimilar principles lead to different classification results. Furthermore, a minimum spanning forest is built, where each tree is rooted on a classification-driven marker and forms a region in the spectral–spatial classification map. Experimental results are presented for two hyperspectral airborne images. The proposed method significantly improves classification accuracies when compared with previously proposed classification techniques.**

***Index Terms*—Classification, hyperspectral images, minimum spanning forest (MSF), multiple classifiers (MCs), segmentation.**

I. Introduction

HYPERSPECTRAL imaging is a relatively recent technique in remote sensing. Acquired remotely by airborne or spaceborne sensors, hyperspectral data are composed of hundreds of spatially coregistered images corresponding to different spectral channels [1], [2]. Fig. 1 shows the structure of a hyperspectral image. Every pixel is presented as a B-dimensional feature vector across the wavelength dimension, called the spectrum of the material in this pixel. This rich information in every spatial location increases the capability to distinguish different physical materials. Thus, hyperspectral imagery opens new perspectives for image classification, which is an important task for a wide variety of applications (precision agriculture, monitoring and management of the environment, and security issues).

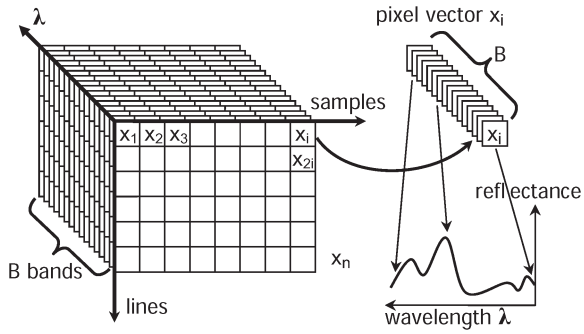

Fig. 1. Structure of a hyperspectral image.

However, such a large number of spectral channels, usually coupled with limited availability of reference data,[1] present challenges to image analysis. While pixelwise classification techniques process each pixel independently without considering information about spatial structures [3]–[6], further improvement of classification results can be achieved by considering spatial dependences between pixels, i.e., by performing spectral–spatial classification [7]–[12].

Segmentation techniques, partitioning an image into homogeneous regions with respect to some criterion of interest (called homogeneity criterion, e.g., intensity or texture), are powerful tools for defining spatial dependences [13]. In previous works, we have distinguished spatial structures in the hyperspectral image by performing unsupervised segmentation [12], [14], [15]. Watershed, partitional clustering, and hierarchical segmentation (HSEG) techniques have been used for this purpose. Segmentation and pixelwise classification were applied independently; then, results were combined using a majority-voting rule (see Fig. 2). Thus, every region from a segmentation map was considered as an adaptive homogeneous neighborhood for all the pixels within this region. The described technique led to a significant improvement of classification accuracies and provided more homogeneous classification maps, when compared with classification techniques using local neighborhoods in order to include spatial information into a classifier.

An alternative way to get accurate segmentation results consists in performing a marker-controlled segmentation [13], [16].

Manuscript received December 30, 2009; revised May 11, 2010. Date of publication September 13, 2010; date of current version October 27, 2010. This work was supported in part by the Marie Curie Research Training Network "HYPER-I-NET."

Y. Tarabalka is with the Faculty of Electrical and Computer Engineering, University of Iceland, 107 Reykjavik, Iceland, and also with the Grenoble Images Speech Signals and Automatics Laboratory (GIPSA-Lab), Grenoble Institute of Technology (INPG), 38402 Saint-Martin-d'Hères Cedex, France (e-mail: yuliya.tarabalka@hyperinet.eu).

J. A. Benediktsson is with the Faculty of Electrical and Computer Engineering, University of Iceland, 107 Reykjavik, Iceland (e-mail: benedikt@hi.is).

J. Chanussot is with the Grenoble Images Speech Signals and Automatics Laboratory (GIPSA-Lab), Grenoble Institute of Technology (INPG), 38402 Saint-Martin-d'Hères Cedex, France (e-mail: jocelyn.chanussot@gipsa-lab.grenoble-inp.fr).

J. C. Tilton is with the NASA Goddard Space Flight Center, Greenbelt, MD 20771 USA (e-mail: james.c.tilton@nasa.gov).

Color versions of one or more of the figures in this paper are available online at http://ieeexplore.ieee.org.

Digital Object Identifier 10.1109/TGRS.2010.2062526

[1]By *reference data*, we mean manually labeled pixels which are used for training classifiers followed by assessment of classification accuracies.

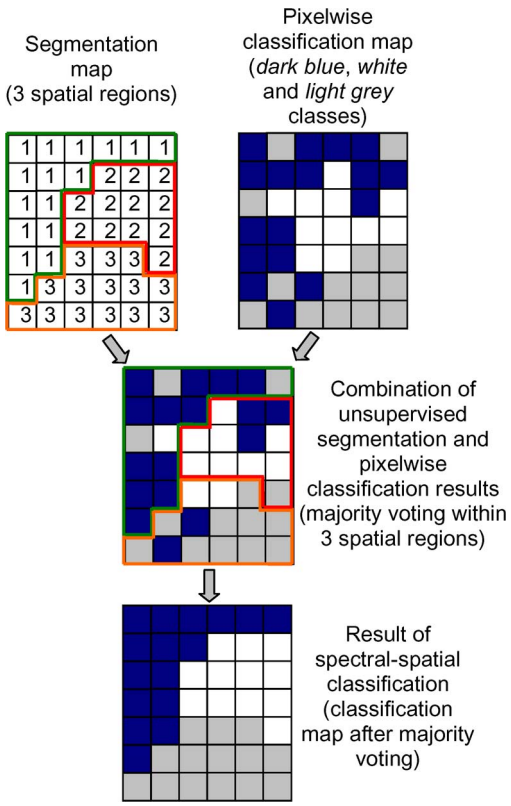

Fig. 2. Example of spectral–spatial classification using majority voting within segmentation regions.

The idea behind this approach is to select, for every spatial object, one or several pixels belonging to this object (called a *region seed*, or a *marker* of the corresponding region) and to grow regions from the selected seeds so that every region in the resulting segmentation map is associated with one region seed. The markers of regions can be chosen either manually or automatically. Recently, we have proposed to use probability estimates obtained by the pixelwise support vector machine (SVM) classification in order to select the most reliable classified pixels as markers, i.e., seeds of spatial regions [17]. Furthermore, image pixels were grouped into a minimum spanning forest (MSF) where each tree was rooted on a classification-derived marker. The decision to connect a pixel, which is not yet in the forest, to one of the trees in the forest was based on its similarity to one of the adjacent pixels already belonging to the forest. By assigning the class of each marker to all the pixels within the region grown from this marker, a spectral–spatial classification map was obtained. The described technique led to a significant improvement of classification accuracies when compared with previously proposed methods. The drawback of this method is that the choice of markers strongly depends on the performances of the selected pixelwise classifier (e.g., the SVM classifier in our previous work [17]).

In this paper, we aim to mitigate the dependence of the marker-selection procedure from the choice of a pixelwise classifier. This can be achieved by using not a single classification algorithm for marker selection but an ensemble of classifiers, i.e., *multiple classifiers (MCs)*. For this purpose, several individual classifiers must be chosen and combined within one system in such a way that the complementary benefits of each classifier are used, while their weaknesses are avoided.

In this paper, a new *marker-selection method* based on an *MC* system is proposed. Several classifiers are used independently to classify an image. Furthermore, a marker map is constructed by selecting the pixels assigned by all the classifiers to the same class. We propose to use spectral–spatial classifiers in the preliminary step of the marker-selection procedure, each of them combining the results of a pixelwise classification and one of the unsupervised segmentation techniques (see Fig. 2). By using spectral–spatial classifiers in this step, spatial context in the image is taken into account, and classification maps are more accurate when compared with pixelwise classification maps. This leads to more accurate marker-selection results. The proposed marker-selection method is incorporated into a new *multiple spectral–spatial classification (MSSC) scheme (MSSC-MSF)* based on the construction of an MSF from region markers (see Fig. 3).

In order to assess the importance of spectral–spatial approaches for marker selection, we have also implemented a *multiple classification scheme (MC-MSF)*. Here, spectral–spatial classification maps are replaced by the maps obtained using pixelwise classification techniques. Finally, a marker map is computed, and an MSF from the selected markers is constructed.

Although the classification approach proposed in this paper has been designed for hyperspectral data, the method is general and can be applied for other types of data as well. Two hyperspectral airborne images are used to demonstrate experimental results: an image recorded by the reflective optics system imaging spectrometer (ROSIS) over the University of Pavia, Italy, and an Airborne Visible/Infrared Imaging Spectrometer (AVIRIS) image acquired over Northwestern Indiana's Indian Pines site [18].

This paper is organized as follows. In the next section, the MC approach is briefly discussed. Section III describes the proposed classification scheme. Experimental results are discussed in Section IV. Finally, conclusions are drawn in Section V.

II. MC Approach

The traditional approach for a pattern recognition problem is to search for the individual algorithm giving the best possible classification performances. However, in many cases, the classification accuracy can be improved by using an ensemble of classifiers, or multiple classifiers. This is due to the fact that, although one of the classification algorithms would yield the best performance, the sets of pixels (patterns, in general) misclassified by the different algorithms would not necessarily overlap. Thus, the aim of an *MC* system is to determine an efficient combination method that makes use of the complementary benefits of each classifier while tackling the individual drawbacks [19]–[21].

A schematic representation of an MC system is shown in Fig. 4. An important issue for an efficient MC system is that the individual classifiers should be independent. More precisely, the classifiers should not agree with each other when they

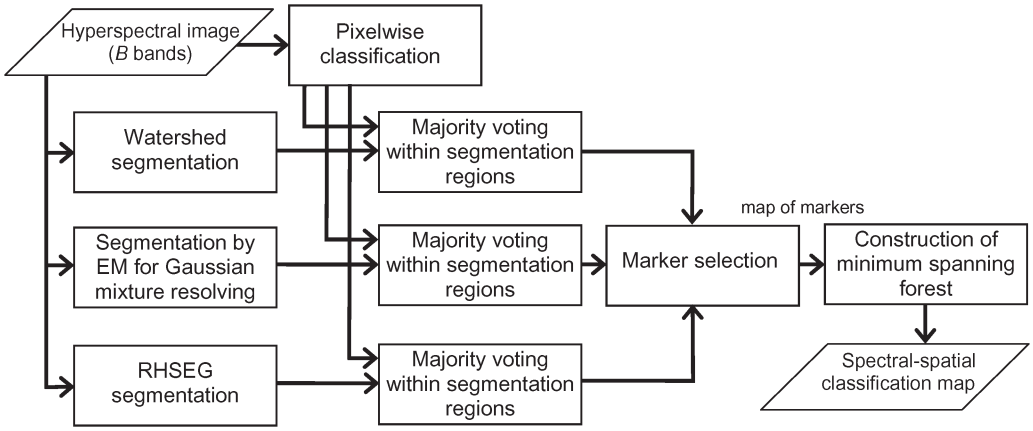

Fig. 3. Flowchart of the proposed *MSSC-MSF* classification scheme.

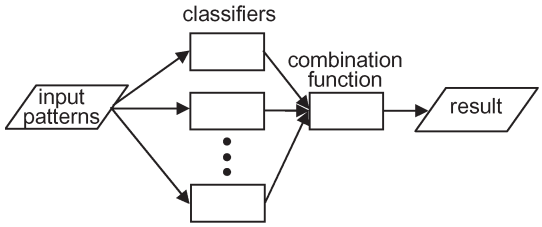

Fig. 4. Schematic diagram of an MC system.

misclassify a pixel [20]. The complementary properties of the different classifiers selected for the MC system should ensure, to a certain extent, this requirement.

Another important issue is the rule for combining the individual classifiers (i.e., combination function). The individual classifier outputs, such as class labels and possible posterior probabilities, are typically combined by voting rules, belief functions, statistical techniques, the Dempster–Shafer evidence theory, and other schemes [19]. For a given pixel, if all the classifiers agree on the same class k, the evident combination rule consists in assigning this pixel to the class k in the final classification map. On the other side, when individual classifiers disagree in assigning the given pixel, the procedure of final decision making is not that straightforward, and different combination functions may yield different results. A typical result of the MC system is a final classification map where each pixel has a unique class label. This type of MC systems has been previously used for remote-sensing image classification [21]–[23].

In this paper, we propose to address the combination-rule issue in the following way: According to the exclusionary rule, only the pixels where all the classifiers agree, i.e., the most reliable pixels, are kept in the classification map. The rest of the pixels are further classified by constructing an MSF rooted on the "reliable" pixels, i.e., by incorporating the spatial information into classification.

Going back to the first issue for designing an MC system, different individual classifiers must be chosen. For instance, standard pixelwise classification algorithms can be used for this purpose, such as SVM, maximum likelihood (*ML*), and k-nearest neighborhood (k-*NN*) methods (parametric and nonparametric techniques based on different principles). We have used these individual techniques in the *MC-MSF* classification scheme. Furthermore, we propose to use spectral–spatial classifiers as individual classifiers for the MC system (*MSSC-MSF* classification scheme), each of them combining the results of a pixelwise classification and one of the unsupervised segmentation techniques. Different segmentation methods based on dissimilar principles lead to different classification results. The use of spectral–spatial classifiers yields more accurate classification maps when compared with those obtained by performing pixelwise classification.

III. Proposed Classification Scheme

The flowchart of the proposed *MSSC-MSF* classification method is shown in Fig. 3. At the input, a B-band hyperspectral image is given, which can be considered as a set of n pixel vectors $\mathbf{X} = \{\mathbf{x}_j \in \mathbb{R}^B, j = 1, 2, \ldots, n\}$. Classification consists in assigning each pixel to one of the K classes of interest. In the following, each step of the proposed procedure is described.

Segmentation can be defined as an exhaustive partitioning of the input image into regions, each of which is considered to be homogeneous with respect to some criterion of interest. We have investigated the use of three techniques for hyperspectral image segmentation, as described hereafter.

A. Watershed Segmentation

Watershed transformation is a powerful morphological approach to image segmentation that combines region growing and edge detection. The watershed is usually applied to the gradient function, and it divides an image into regions so that each region is associated with one minimum of the gradient image [24].

The extension of a watershed technique to the case of hyperspectral images has been investigated in [15] and [25]. In this paper, we present watershed results obtained by the scheme we proposed and described in [15]: First, a one-band robust color morphological gradient (CMG) (RCMG) [26] for the hyperspectral image is computed.

For each pixel vector $\mathbf{x}_p$, let $\chi = [\mathbf{x}_p^1, \mathbf{x}_p^2, \ldots, \mathbf{x}_p^e]$ be a set of e vectors contained within a structuring element E (i.e., the

pixel $\mathbf{x}_p$ itself and $e-1$ neighboring pixels). A 3×3 square structuring element with the origin at its center is typically used. The *CMG*, using the Euclidean distance, is computed as

$$\mathrm{CMG}_E(\mathbf{x}_p) = \max_{i,j \in \chi} \left\{ \left\| \mathbf{x}_p^i - \mathbf{x}_p^j \right\|_2 \right\} \quad (1)$$

i.e., the maximum of the distances between all pairs of vectors in the set χ. One of the drawbacks of the CMG is that it is very sensitive to noise. To overcome the problem of outliers, the RCMG has been proposed [26]. The scheme to make a CMG robust consists of removing the two pixels that are furthest apart and then finding the CMG of the remaining pixels. This process can be repeated several times until a good estimate of the gradient is obtained.

Thus, the *RCMG*, using the Euclidean distance, can be defined as

$$\mathrm{RCMG}_E(\mathbf{x}_p) = \max_{i,j \in [\chi - REM_r]} \left\{ \left\| \mathbf{x}_p^i - \mathbf{x}_p^j \right\|_2 \right\} \quad (2)$$

where REM_r is a set of r vector pairs removed. If E is a 3×3 square structuring element, $r = 1$ is recommended [26].

Furthermore, watershed transformation is applied on the gradient image using a standard algorithm [27]. As a result, the image is partitioned into a set of regions and one subset of watershed pixels, i.e., pixels situated on the borders between regions. Finally, every watershed pixel is assigned to the neighboring region with the "closest" median[2] (the distance between the vector median of this region and the watershed pixel is minimal).

B. Segmentation by EM

The expectation maximization (EM) algorithm for the Gaussian mixture resolving belongs to the group of partitional-clustering techniques [14], [29]. The use of partitional clustering for hyperspectral image segmentation has been discussed in [14]. Clustering aims at finding groups of spectrally similar pixels. We assume that pixels belonging to the same cluster are drawn from a multivariate Gaussian probability distribution. Each image pixel can be statistically modeled by the following probability density function:

$$p(\mathbf{x}) = \sum_{c=1}^{C} \omega_c \phi_c(\mathbf{x}\boldsymbol{\mu}_c, \boldsymbol{\Sigma}_c) \quad (3)$$

where C is the number of clusters, $\omega_c \in [0,1]$ is the mixing proportion (weight) of cluster c with $\sum_{c=1}^{C} \omega_c = 1$, and $\phi(\boldsymbol{\mu}, \boldsymbol{\Sigma})$ is the multivariate Gaussian density with mean $\boldsymbol{\mu}$ and covariance matrix $\boldsymbol{\Sigma}$

$$\phi_c(\mathbf{x}\boldsymbol{\mu}_c, \boldsymbol{\Sigma}_c) = \frac{1}{(2\pi)^{B/2}} \frac{1}{|\boldsymbol{\Sigma}_c|^{1/2}} \exp\left\{ -\frac{1}{2} (\mathbf{x} - \boldsymbol{\mu}_c)^T \boldsymbol{\Sigma}_c^{-1} (\mathbf{x} - \boldsymbol{\mu}_c) \right\}. \quad (4)$$

[2]A standard vector median [28] for the region $\mathbf{S} = \{\mathbf{s}_j \in \mathbb{R}^B, j = 1, 2, \ldots, l\}$ is defined as $\mathbf{s}_{VM} = \arg\min_{\mathbf{s} \in \mathbf{S}} \{\sum_{j=1}^{l} \|\mathbf{s} - \mathbf{s}_j\|_1\}$.

The parameters of the distributions $\boldsymbol{\psi} = \{C, \omega_c, \boldsymbol{\mu}_c, \boldsymbol{\Sigma}_c; c = 1, 2, \ldots, C\}$ are estimated by the EM algorithm, as described in [14]. An upper bound on the number of clusters, which is a required input parameter, is recommended to be chosen as slightly superior to the number of classes.

When the algorithm converges, the partitioning of the set of image pixels into clusters is obtained. However, as no spatial information is used during the clustering procedure, pixels with the same cluster label can form a connected spatial region or can belong to disjoint regions. In order to obtain a segmentation map, a connected component-labeling algorithm [30] is applied to the output image partitioning obtained by clustering.

The total number of parameters to be estimated by the EM algorithm is $P = (B(B+1)/2 + B + 1)C + 1$, where B is a dimensionality of feature vectors. If the value of B is large, P may be quite a large number. This may cause a problem of the covariance-matrix singularity or inaccurate parameter estimation results. In order to avoid these problems, we propose to previously apply a feature reduction using the method of piecewise constant function approximations (*PCFAs*) [31], which has shown good performances for hyperspectral data feature extraction.

C. RHSEG Segmentation

The HSEG algorithm is a segmentation technique based on iterative hierarchical stepwise optimization region-growing method. Furthermore, it provides a possibility of merging nonadjacent regions by spectral clustering [32].

The following outline of the HSEG algorithm is based on the description given in [32] and [33]

1) Initialize the segmentation by assigning for each pixel a region label. If a presegmentation is provided, label each pixel according to the presegmentation. Otherwise, label each pixel as a separate region.
2) Calculate the dissimilarity criterion value between all pairs of spatially adjacent regions.
3) Find the smallest dissimilarity criterion value $dissim\_val$ and set $thresh\_val$ equal to it. Then, merge all pairs of spatially adjacent regions with $dissim\_val = thresh\_val$.
4) If a parameter $S_{\mathrm{wght}} > 0.0$, merge all pairs of spatially nonadjacent regions with $dissim\_val \leq S_{\mathrm{wght}} \cdot thresh\_val$.
5) If convergence is not achieved, go to step 2).

In order to reduce computational demands, a recursive divide-and-conquer approximation of HSEG (RHSEG) has been developed. The NASA Goddard RHSEG software provides an efficient implementation of the RHSEG algorithm.

When determining most similar pair of regions, we propose to choose the standard Spectral Angle Mapper (SAM) between the region mean vectors and as a dissimilarity criterion [32]. The SAM measure between $\mathbf{u}_i$ and $\mathbf{u}_j$ $(\mathbf{u}_i, \mathbf{u}_j \in \mathbb{R}^B)$

determines the spectral similarity between two vectors by computing the angle between them. It is defined as

$$\mathrm{SAM}(\mathbf{u}_i, \mathbf{u}_j) = \arccos\left(\frac{\sum_{b=1}^{B} u_{ib}u_{jb}}{\left[\sum_{b=1}^{B} u_{ib}^2\right]^{1/2}\left[\sum_{b=1}^{B} u_{jb}^2\right]^{1/2}}\right). \quad (5)$$

The optional parameter S_{wght} tunes the relative importance of spectral clustering *versus* region growing. If $S_{\mathrm{wght}} = 0.0$, only merging of spatially adjacent regions is performed. If $0.0 < S_{\mathrm{wght}} \leq 1.0$, merging between spatially adjacent regions is favored compared with merging of spatially nonadjacent regions by a factor of $1.0/S_{\mathrm{wght}}$. As discussed in [34], the optimal parameter S_{wght} can be chosen based on *a priori* knowledge about information classes contained in the image. If some classes have very similar spectral responses, we recommended to choose $S_{\mathrm{wght}} = 0.0$ or close to this value.[3] Otherwise, we recommend increasing the possibility of merging spatially nonadjacent regions. If $S_{\mathrm{wght}} > 0.0$, labeling of connected components has to be applied after RHSEG in order to obtain a segmentation map where each spatially connected component has a unique label.

RHSEG provides as output a hierarchical sequence of image partitions. In this sequence, a particular object can be represented by several regions at finer levels of details and can be assimilated with other objects in one region at coarser levels of details. This hierarchical sequence allows flexibility in choosing the appropriate level of detail for the segmentation map. When training data are available, it is a simple process to quantitatively evaluate the segmentation results at each hierarchical level versus the training data to select the appropriate level of detail. Otherwise, an appropriate level of segmentation detail can be chosen interactively with the program HSEGViewer [32], or an automated method, tailored to the application, can be developed, such as that explored in [35].

D. Pixelwise Classification

Independent of the previous steps, a pixelwise classification of the hyperspectral image is performed. We propose to use an SVM classifier for this purpose. Other pixelwise classifiers could be used. However, SVMs perform extremely well in classifying high-dimensional data when a limited number of training samples are available [5], [36]. We refer the reader to [5] and [37] for details on SVM technique. This step results in a classification map where each pixel has a unique class label.

E. Majority Voting Within Segmentation Regions

Each of the obtained unsupervised segmentation maps is combined with the pixelwise classification map using the majority-voting principle: For every region in the segmentation map, all the pixels are assigned to the most frequent class within this region (see an illustrative example in Fig. 2). Thus, q segmentation maps combined with the pixelwise classification map result in q spectral–spatial classification maps (since we propose to use three different segmentation techniques, in this particular case, $q = 3$).

F. Marker Selection

This step consists of computing a map of markers using spectral–spatial classification maps from the previous step and the exclusionary rule: For every pixel, if all the classifiers agree, the pixel is kept as a marker with a corresponding class label. The resulting map of m markers contains the most reliably classified pixels.

G. Construction of a MSF

In the final step, image pixels are grouped into an MSF rooted on the selected markers [17]. Each pixel is considered as a vertex $v \in V$ of an undirected graph $G = (V, E, W)$, where V and E are the sets of vertices and edges, respectively, and W is a mapping of the set of the edges E into $\mathbb{R}^+$. Each edge $e_{i,j} \in E$ of this graph connects a couple of vertices i and j corresponding to the neighboring pixels. Furthermore, a weight $w_{i,j}$ is assigned to each edge $e_{i,j}$, which indicates the degree of dissimilarity between two vertices (i.e., two corresponding pixels) connected by this edge. We propose to use an eight-neighborhood and the SAM measure for computing the weights of edges, as described in [17].

Given a graph $G = (V, E, W)$, the *MSF* rooted on a set of m distinct vertices $\{t_1, \ldots, t_m\}$ consists in finding a spanning forest $F^* = (V, E_{F^*})$ of G such that each distinct tree of F^* is grown from one root t_i, and the sum of the edges' weights of F^* is minimal [38]

$$F^* \in \arg\min_{F \in SF}\left\{\sum_{e_{i,j} \in E_F} w_{i,j}\right\} \quad (6)$$

where SF is a set of all spanning forests of G rooted on $\{t_1, \ldots, t_m\}$.

Algorithm 1 Prim's Algorithm
Require: Connected graph $G = (V, E, W)$
Ensure: Tree $T^* = (V^*, E^*, W^*)$
  $V^* = \{v\}$, v is an arbitrary vertex from V
  while $V^* \neq V$ **do**
    Choose edge $e_{i,j} \in E$ with minimal weight such that $i \in V^*$ and $j \notin V^*$
    $V^* = V^* \cup \{j\}$
    $E^* = E^* \cup \{e_{i,j}\}$
  end while

In order to obtain the MSF rooted on m markers corresponding to the vertices t_i, $i = 1, \ldots, m$, an additional root vertex r is added and is connected by the null-weight edges to the vertices t_i. The minimum spanning tree of the constructed graph induces an MSF in G, where each tree is grown on a

[3]The analysis reported in this paper was performed with version 1.40 of the RHSEG software. The recently released version 1.50 of RHSEG produces similar segmentation results, except that it can exhibit improved results for larger values of S_{wght}, particularly for data sets containing classes with mostly dissimilar spectral responses.

TABLE I
CLASSIFICATION ACCURACIES IN PERCENT FOR THE *University of Pavia* IMAGE: OA, AA, KAPPA COEFFICIENT (κ), AND CLASS-SPECIFIC ACCURACIES

	3-NN	ML	SVM	ECHO	WH+MV	EM+MV	RHSEG +MV	SVMMSF +MV	MC-MSF	MSSC-MSF
OA	68.38	79.06	81.01	87.58	85.42	94.00	93.85	91.08	87.98	**97.90**
AA	77.21	84.85	88.25	92.16	91.31	93.13	97.07	94.76	92.05	**98.59**
κ	59.85	72.90	75.86	83.90	81.30	91.93	91.89	88.30	84.32	**97.18**
Asphalt	64.96	76.43	84.93	87.98	93.64	90.10	94.77	93.16	87.01	**98.00**
Meadows	63.18	75.99	70.79	81.64	75.09	95.99	89.32	85.65	83.24	**96.67**
Gravel	62.31	64.57	67.16	76.91	66.12	82.26	96.14	89.15	75.37	**97.80**
Trees	95.95	97.08	97.77	**99.31**	98.56	85.54	98.08	91.24	98.97	98.83
Metal sheets	99.73	99.91	99.46	99.91	99.91	**100**	99.82	99.91	99.91	99.91
Bare soil	57.42	70.03	92.83	93.96	97.35	96.72	99.76	99.91	93.24	**100**
Bitumen	82.67	90.62	90.42	92.97	96.23	91.85	**100**	98.57	95.11	99.90
Bricks	77.08	90.10	92.78	97.35	97.92	98.34	99.29	99.05	97.00	**99.76**
Shadows	91.57	98.87	98.11	**99.37**	96.98	97.36	96.48	96.23	98.62	96.48

vertex t_i; the MSF is obtained after removing the vertex r. Prim's algorithm can be used for building the MSF (see Algorithm 1) [39]. The efficient implementation of the algorithm using a binary min-heap is possible [40]; the resulting time complexity of the algorithm is $O(|E|\log|V|)$. Finally, a spectral–spatial classification map is obtained by assigning the class of each marker to all the pixels grown from this marker.

IV. EXPERIMENTAL RESULTS AND DISCUSSION

Two different hyperspectral images were used for the experiments with different contexts (one urban area and one agricultural area) and recorded by different sensors (ROSIS and AVIRIS). These data sets and the corresponding results are discussed in the next two sections.

A. Classification of the University of Pavia Image

The *University of Pavia* image was recorded by the ROSIS optical sensor over the urban area of the University of Pavia, Italy. The image is 610 × 340 pixels with a spatial resolution of 1.3 m/pixel. The number of data channels in the acquired image is 115 (with a spectral range from 0.43 to 0.86 μm). The 12 most noisy channels have been removed, and the remaining 103 bands were used for the experiments. Nine classes of interest are considered, which are detailed in Table I. Fig. 5 shows a three-band false color image and the reference data. The training and test sets are composed of 3921 and 40 002 pixels, respectively. More information about the image, with the number of training and test samples for each class can be found in [14].

The segmentation of the considered image was performed using the three different techniques discussed in the previous section. For the EM algorithm, the maximum number of clusters was chosen to be equal to ten (typically slightly superior to the number of classes). Before applying the EM technique, a feature extraction on the original 103-band image was applied using the method of PCFA [31] to get a ten-band image $\mathbf{Y}_{UP}$. Pixels from the training set were used for selecting features. The method produced an averaging of the following groups of adjacent spectral channels: 1–4, 5–10, 11–24, 25–35, 36–43, 44–68, 69–72, 73–75, 76–79, and 80–103.

For the RHSEG algorithm, we chose $S_{\text{wght}} = 0.1$ since the image of this urban area contains classes with mostly dissimilar spectral responses. A segmentation map at an appropriate level of segmentation detail was chosen interactively with the program HSEGViewer. The obtained watershed, EM, and RHSEG segmentation maps contained 11 802, 22 549, and 7575 regions, respectively.

The multiclass pairwise SVM classification, with the Gaussian radial basis function (RBF) kernel, of the original image was performed with the parameters chosen by fivefold cross validation: $C = 128$ and $\gamma = 0.125$. The results of the pixelwise classification were combined with the segmentation results using the majority voting approach. Finally, the marker selection (see Fig. 5(g); 132 521, i.e., 64% of pixels were selected as markers) and the construction of an MSF were performed, resulting in the *MSSC-MSF* spectral–spatial classification map shown in Fig. 5(h).

Table I summarizes the global and class-specific accuracies of the pixelwise SVM, segmentation plus majority voting (*WH + MV*, *EM + MV*, *RHSEG + MV* for three segmentation techniques, respectively), and the proposed *MSSC-MSF* classification methods. The following measures of accuracy were used: Overall accuracy [(OA) is the percentage of correctly classified pixels], average accuracy [(AA) is the mean of class-specific accuracies, i.e., the percentage of correctly classified pixels for each class], and kappa coefficient (κ is the percentage of agreement, i.e., correctly classified pixels, corrected by the number of agreements that would be expected purely by chance [41]). In order to compare the performances of the proposed technique with the previously proposed methods, we have also included results of the well-known ECHO spatial classifier [7], as well as the results obtained using the construction of an MSF from the probabilistic SVM-derived markers followed by majority voting within connected regions *(SVMMSF + MV)* [17].

In addition, we assessed the importance of spectral–spatial approaches for marker selection. For this purpose we replaced the *WH + MV*, *EM + MV*, and *RHSEG + MV* classification maps by three maps obtained using standard pixelwise classification techniques (we call this modified scheme an *MC-MSF* classification method). SVM, *ML*, and three-nearest neighborhood (3-*NN*, using the SAM distance) methods were used for this purpose. The ML and the 3-NN techniques were applied on the ten-band image $\mathbf{Y}_{UP}$ feature vectors. The accuracies of the modified *MC-MSF* classification as well as the pixelwise classification results are given in Table I.

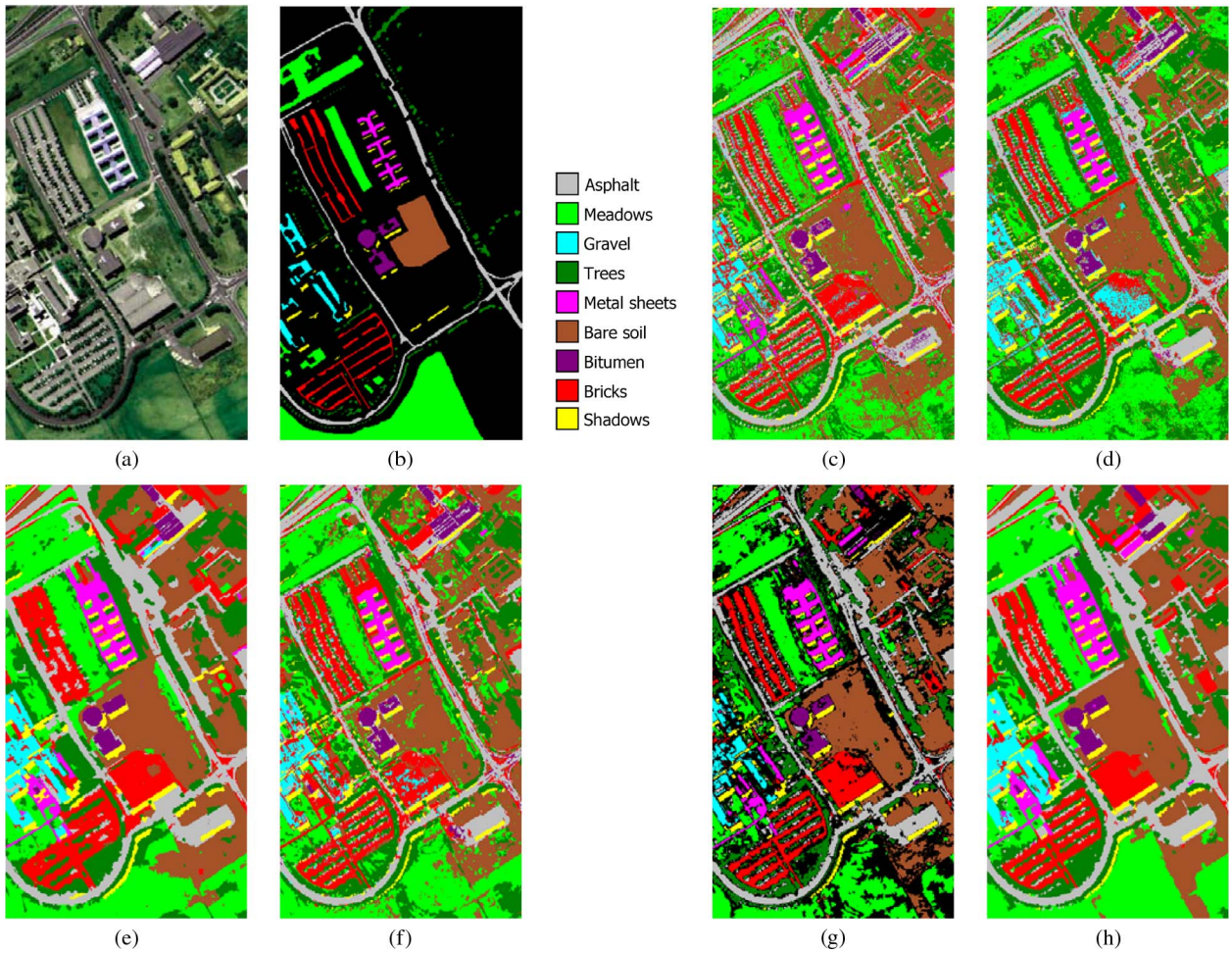

Fig. 5. *University of Pavia* image. (a) Three-band color composite. (b) Reference data: Asphalt, meadows, gravel, trees, metal sheets, bare soil, bitumen, bricks, and shadows. (c) SVM pixelwise classification map. (d) *ECHO* classification map. (e) *SVMMSF + MV* classification map. (f) *MC-MSF* classification map. (g) *MSSC-MSF* marker map. (h) *MSSC-MSF* classification map.

As can be seen from Table I, the SVM method gives the highest accuracies among all the pixelwise classification techniques. All the spectral–spatial approaches yield higher classification accuracies when compared with pixelwise methods. The proposed MC approach for marker selection improves the accuracies when compared with those obtained by classification techniques used in the preliminary step of the marker-selection procedure, both for the *MC-MSF* and *MSSC-MSF* methods. The best global and the best class-specific accuracies for most classes are achieved by applying the proposed *MSSC-MSF* method. According to the results of the McNemar's test [42], the *MSSC-MSF* classification map is significantly more accurate when compared with those obtained by other classification approaches, using 5% level of significance. In this case, the OA is improved by 16.9 percentage points and the AA is improved by 10.3 percentage points when compared with the SVM classification. All the class-specific accuracies are higher than 96%. Only the accuracy for the class *shadows*, representing small spatial structures, is slightly reduced when compared with the SVM results (the drawback of applying spectral–spatial classification to small structures was discussed, for instance, in [14]). The *MSSC-MSF* classification accuracies are much higher than the *MC-MSF* accuracies. Furthermore, the presented classification accuracies are higher than all previous results we have found in the literature for the same data.

Fig. 5 shows the *MC-MSF* and *MSSC-MSF* classification maps, as well as the SVM, *ECHO*, and *SVMMSF + MV* classification maps given for comparison. In Fig. 5(g) [*MSSC-MSF* marker map], it can be seen that the marker pixels, i.e., the most reliable classified pixels, are typically located at the center of spatial structures, while borders of structures are under a high risk of being misclassified. The *MSSC-MSF* classification map [see Fig. 5(h)] contains much more homogeneous regions when compared with the maps obtained by other pixelwise and spectral–spatial approaches. These results prove the importance of the use of MC systems and spatial information throughout the classification procedure.

B. Classification of the Indian Pines Image

The proposed scheme was also tested on the *Indian Pines* image of a vegetation area, acquired by the AVIRIS sensor over the Indian Pines site in Northwestern Indiana. The image has spatial dimensions of 145 by 145 pixels, with a spatial resolution of 20 m/pixel. Twenty water absorption bands

TABLE II
CLASSIFICATION ACCURACIES IN PERCENT FOR THE *Indian Pines* IMAGE: OA, AA, KAPPA COEFFICIENT (κ), AND CLASS-SPECIFIC ACCURACIES

	3-NN	ML	SVM	ECHO	WH+MV	EM+MV	RHSEG +MV	SVMMSF +MV	MC-MSF	MSSC-MSF
OA	66.27	75.41	78.17	82.64	86.63	83.60	90.86	91.80	86.66	**92.32**
AA	76.77	79.61	85.97	83.75	91.61	85.34	93.96	**94.28**	92.58	94.22
κ	62.04	72.25	75.33	80.38	84.83	81.43	89.56	90.64	84.82	**91.19**
Corn-no till	41.84	71.39	78.18	83.45	**94.22**	89.09	90.46	93.21	83.82	89.74
Corn-min till	62.24	63.01	69.64	75.13	78.06	75.64	83.04	**96.56**	74.62	86.99
Corn	73.37	85.87	91.85	92.39	88.59	65.22	95.65	95.65	**96.74**	95.11
Soybeans-no till	67.43	79.43	82.03	90.10	**96.30**	88.14	92.06	93.91	93.36	91.84
Soybeans-min till	53.91	52.65	58.95	64.14	68.82	65.67	84.04	81.97	72.91	**89.16**
Soybeans-clean till	64.72	85.99	87.94	89.89	90.78	95.04	95.39	97.16	95.92	**97.34**
Alfalfa	84.62	48.72	74.36	48.72	**94.87**	**94.87**	92.31	**94.87**	**94.87**	**94.87**
Grass/pasture	86.35	93.51	92.17	94.18	95.08	93.96	94.41	94.63	**98.21**	94.63
Grass/trees	91.97	94.69	91.68	96.27	**97.99**	96.41	97.56	97.27	97.70	97.85
Grass/pasture-mowed	**100**	36.36	**100**	36.36	**100**	**100**	**100**	**100**	**100**	**100**
Hay-windrowed	95.67	97.72	97.72	97.72	99.54	99.32	99.54	**99.77**	99.54	**99.77**
Oats	80.00	**100**	**100**	**100**	**100**	40.00	**100**	**100**	**100**	**100**
Wheat	**99.38**	98.15	98.77	98.15	**99.38**	98.77	98.15	**99.38**	**99.38**	**99.38**
Woods	86.17	95.42	93.01	94.21	97.11	96.70	98.63	**99.68**	98.47	99.44
Bldg-Grass-Tree-Drives	45.15	73.03	61.52	81.52	69.39	66.67	**82.12**	68.79	77.88	73.64
Stone-steel towers	95.56	97.78	97.78	97.78	95.56	**100**	**100**	95.56	97.78	97.78

(104–108, 150–163, and 220) have been removed [18], and a 200-band image was used for the experiments. The reference data contain sixteen classes of interest, which represent mostly different types of crops and are detailed in Table II. A three-band false-color image and the reference data are shown in Fig. 6. We have randomly chosen 50 samples for each class from the reference data as training samples, except for classes *"alfalfa," "grass/pasture mowed,"* and *"oats."* These classes contain a small number of samples in the reference data. Therefore, only 15 samples for each of these classes were chosen randomly to be used as training samples. The remaining samples composed the test set.

Segmentation of the *Indian Pines* image was performed using the three discussed techniques. For the EM technique, the upper bound on the number of classes was chosen to be equal to 17, and a feature reduction has been previously applied using the method of PCFA [31] to get a ten-band image $\mathbf{Y}_{IN}$. The following groups of bands were averaged: 1–18, 19–36, 37–53, 54–57, 58–61, 62–75, 76–81, 82–99, 100–140, and 141–200.

Since some classes have very similar spectral responses in the *Indian Pines* image (for instance, three classes of corn and three classes of soybeans), we set $S_{\mathrm{wght}} = 0.0$ for the RHSEG method. A segmentation map at the relevant level of hierarchy was chosen with the program HSEGViewer. The resulting watershed, EM, and RHSEG segmentation maps contained 1277, 3832, and 823 regions, respectively.

A pixelwise classification on the 200-band image was performed using the multiclass one *versus* one SVM classifier with the Gaussian RBF kernel. The optimal parameters C and γ were chosen by fivefold cross validation: $C = 128$ and $\gamma = 2^{-6}$. After the segmentation results were combined with the pixelwise classification map, the marker selection (14 409, i.e., 68% of the pixels, were selected as markers) and the MSF construction were applied, as described in the previous section.

Table II gives the global and class-specific accuracies of the pixelwise SVM segmentation, followed by majority voting and the proposed *MSSC-MSF* classification techniques. The performances of the proposed approach are compared with those obtained by the ECHO and *SVMMSF + MV* methods, as described in the previous section. Finally, the *MC-MSF* classification was applied in the same way as for the previous data set.

From the table, similar conclusions as with the previous data set can be derived. The SVM classification yields the best accuracies among all the applied pixelwise methods. The spectral–spatial classification accuracies are always higher when compared with the pixelwise accuracies. The proposed MC method succeeds in combining several classification results for further improvement of accuracies. The *MSSC-MSF* yields the best OA, kappa coefficient, and most of the class-specific accuracies. The AA is only slightly (nonsignificantly) lower when compared with that obtained by the recently proposed *SVMMSF + MV* method. Following the results of the McNemar's test, the *MSSC-MSF* and *SVMMSF + MV* accuracies are not significantly different using 5% level of significance. These two techniques significantly outperform other classification approaches.

Fig. 6 shows the SVM, *MC-MSF*, *MSSC-MSF*, and *SVMMSF + MV* classification maps. As can be seen, the *MSSC-MSF* map contains much more homogeneous spatial structures when compared with the SVM and *MC-MSF* maps and is comparable with the *SVMMSF + MV* map. Again, spectral–spatial marker-based techniques yielded the most accurate classification maps.

Although for the *Indian Pines* image, the *MSSC-MSF* and *SVMMSF + MV* methods yield similar results, here, we stress the advantages of the proposed *MSSC-MSF* approach *versus* the previous one for spectral–spatial classification.

1) *Robustness*: While for the *SVMMSF + MV* method, the marker selection strongly depends on the performances of the selected pixelwise classifier, the MC approach mitigates this dependence. Since in the *MSSC-MSF* scheme, different segmentation maps are combined with one pixelwise classification map, the choice of the classifier is also important. However, if in the *SVMMSF + MV* method, a pixel was wrongly classified with a high probability, it will yield a wrong marker. In the new approach, the majority voting within segmentation regions

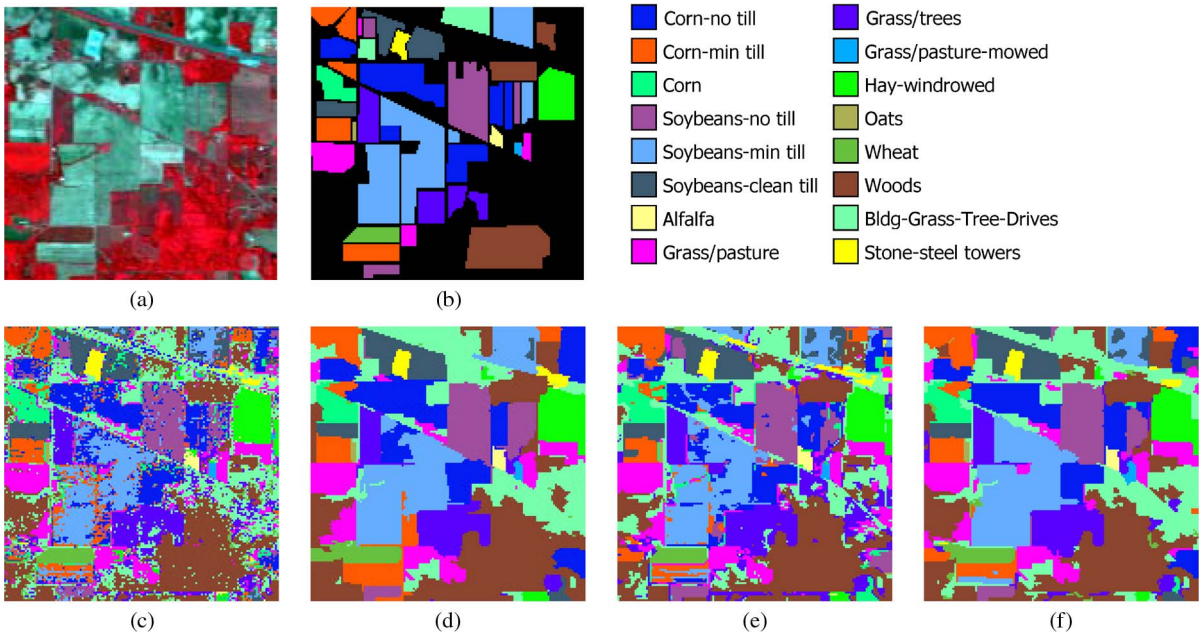

Fig. 6. *Indian Pines* image. (a) Three-band color composite. (b) Reference data: Corn-no till, Corn-min till, Corn, Soybeans-no till, Soybeans-min till, Soybeans-clean till, Alfalfa, Grass/pasture, Grass/trees, Grass/pasture-mowed, Hay-windrowed, Oats, Wheat, Woods, Bldg-Grass-Tree-Drives, Stone-steel towers. (c) SVM pixelwise classification map. (d) *SVMMSF + MV* classification map. (e) *MC-MSF* classification map. (f) *MSSC-MSF* classification map.

can correct the misclassification result for a particular pixel before the marker map is built.

2) *Computational Complexity*: In the *SVMMSF + MV* method, the probabilistic pixelwise SVM classification part is the most time consuming [43]. In the *MSSC-MSF* approach, SVM classification is performed without the computation of probability estimates; this reduces the pixelwise classification-part execution time. The unsupervised segmentation techniques are much less time consuming when compared with the SVM classification. Furthermore, their efficient implementations are available, and they can be executed in parallel at the same time with the SVM classification. As a conclusion, the efficient implementation of the proposed *MSSC-MSF* approach is possible, which would run faster than the previously proposed *MSSC-MSF* method.

V. Conclusion

Hyperspectral sensors capture images in hundreds of narrow spectral channels. The detailed spectral signatures for each spatial location provide rich information about an image scene, leading to better discrimination between physical materials and objects. However, interpretation of these high-dimensional signatures is a challenging task. Although pixelwise classification techniques have given high classification accuracies when dealing with hyperspectral data, the incorporation of the spatial context into classification procedures yields further improvement of the accuracies.

In this paper, a new method for spectral–spatial classification of hyperspectral images based on multiple classifiers has been proposed. First, a marker map is constructed by selecting the pixels assigned by several spectral–spatial classifiers to the same class. This ensures a robust and reliable selection. Then, an MSF rooted on the selected markers is built. Experimental results demonstrated that the proposed method improves classification accuracies, when compared with previously proposed classification schemes, and provides classification maps with homogeneous regions.

In conclusion, the proposed methodology succeeded in taking advantage of multiple classifiers and the spatial and spectral information simultaneously for accurate hyperspectral image classification. The method yields accurate results for different data sets, i.e., data containing large spatial structures and/or small and complex structures, with spectrally dissimilar and/or spectrally confusing classes. Furthermore, its efficient implementation is possible.

While performing particularly well for classification of homogeneous regions, the proposed approach has a drawback common to most of spectral–spatial techniques: It produces a smoother classification map when compared with pixelwise ones and therefore, it risks impairing results near the borders between regions (where mixed pixels[4] are often encountered) or in textured areas. Spectral unmixing techniques [44] can be used for accurate analysis of region borders, while segmentation in the sense of texture [45] can be applied for textured regions.

In the future, we will further explore the integration of spectral–spatial approaches in MC systems for accurate and robust classification of hyperspectral images. Since the incorporation of the spatial information in classification significantly improves accuracies, it is of interest to further

[4]A mixed pixel is defined as a pixel whose value represents the average energy emitted or reflected from several different surfaces occurring within the spatial area represented by the pixel.

investigate performances of the proposed spectral–spatial approaches when a very limited number of training samples are available.

ACKNOWLEDGMENT

The authors would like to thank P. Gamba from the University of Pavia, Italy, and D. Landgrebe from Purdue University, U.S., for providing the hyperspectral data.

REFERENCES

[1] C.-I Chang, *Hyperspectral Data Exploitation: Theory and Applications*. New York: Wiley-Interscience, 2007.

[2] R. O. Green, M. L. Eastwood, C. M. Sarture, T. G. Chrien, M. Aronsson, B. J. Chippendale, J. A. Faust, B. E. Pavri, C. J. Chovit, M. S. Solis, M. R. Olah, and O. Williams, "Imaging spectroscopy and the Airborne Visible Infrared Imaging Spectrometer (AVIRIS)," *Remote Sens. Environ.*, vol. 65, no. 3, pp. 227–248, Sep. 1998.

[3] D. A. Landgrebe, *Signal Theory Methods in Multispectral Remote Sensing*. New York: Wiley, 2003.

[4] P. K. Goel, S. O. Prasher, R. M. Patel, J. A. Landry, R. B. Bonnell, and A. A. Viau, "Classification of hyperspectral data by decision trees and artificial neural networks to identify weed stress and nitrogen status of corn," *Comput. Electron. Agric.*, vol. 39, no. 2, pp. 67–93, May 2003.

[5] G. Camps-Valls and L. Bruzzone, "Kernel-based methods for hyperspectral image classification," *IEEE Trans. Geosci. Remote Sens.*, vol. 43, no. 6, pp. 1351–1362, Jun. 2005.

[6] J.-M. Yang, P.-T. Yu, and B.-C. Kuo, "A nonparametric feature extraction and its application to nearest neighbor classification for hyperspectral image data," *IEEE Trans. Geosci. Remote Sens.*, vol. 48, no. 3, pp. 1279–1293, Mar. 2010.

[7] R. L. Kettig and D. A. Landgrebe, "Classification of multispectral image data by extraction and classification of homogeneous objects," *IEEE Trans. Geosci. Electron.*, vol. GE-14, no. 1, pp. 19–26, Jan. 1976.

[8] A. Farag, R. Mohamed, and A. El-Baz, "A unified framework for MAP estimation in remote sensing image segmentation," *IEEE Trans. Geosci. Remote Sens.*, vol. 43, no. 7, pp. 1617–1634, Jul. 2005.

[9] M. Fauvel, "Spectral and spatial methods for the classification of urban remote sensing data," Ph.D. dissertation, Grenoble Inst. Technol., Grenoble, France, 2007.

[10] M. Fauvel, J. Chanussot, J. A. Benediktsson, and J. R. Sveinsson, "Spectral and spatial classification of hyperspectral data using SVMs and morphological profiles," *IEEE Trans. Geosci. Remote Sens.*, vol. 46, no. 10, pp. 3804–3814, Oct. 2008.

[11] R. Gaetano, G. Moser, G. Poggi, G. Scarpa, and S. B. Serpico, "Region-based classification of multisensor optical-SAR images," in *Proc. IGARSS*, Boston, MA, 2008, pp. IV-81–IV-84.

[12] Y. Tarabalka, J. A. Benediktsson, and J. Chanussot, "Classification of hyperspectral data using support vector machines and adaptive neighborhoods," in *Proc. 6th EARSeL SIG IS Workshop*, Tel Aviv, Israel, 2009.

[13] R. Gonzalez and R. Woods, *Digital Image Processing,* 2nd ed. Englewood Cliffs, NJ: Prentice-Hall, 2002.

[14] Y. Tarabalka, J. A. Benediktsson, and J. Chanussot, "Spectral-spatial classification of hyperspectral imagery based on partitional clustering techniques," *IEEE Trans. Geosci. Remote Sens.*, vol. 47, no. 8, pp. 2973–2987, Aug. 2009.

[15] Y. Tarabalka, J. Chanussot, J. A. Benediktsson, J. Angulo, and M. Fauvel, "Segmentation and classification of hyperspectral data using watershed," in *Proc. IGARSS*, Boston, MA, 2008, pp. III-652–III-655.

[16] P. Soille, *Morphological Image Analysis,* 2nd ed. Berlin, Germany: Springer-Verlag, 2003.

[17] Y. Tarabalka, J. Chanussot, and J. A. Benediktsson, "Segmentation and classification of hyperspectral images using minimum spanning forest grown from automatically selected markers," *IEEE Trans. Syst., Man, Cybern. B, Cybern.*, vol. 40, no. 5, pp. 1267–1279, Oct. 2010.

[18] S. Tadjudin and D. A. Landgrebe, "Covariance estimation with limited training samples," *IEEE Trans. Geosci. Remote Sens.*, vol. 37, no. 4, pp. 2113–2118, Jul. 1999.

[19] L. Xu, A. Krzyzak, and C. Y. Suen, "Methods of combining multiple classifiers and their applications to handwriting recognition," *IEEE Trans. Syst., Man, Cybern.*, vol. 22, no. 3, pp. 418–435, May/Jun. 1992.

[20] J. Kittler, M. Hatef, R. P. W. Duin, and J. Matas, "On combining classifiers," *IEEE Trans. Pattern Anal. Mach. Intell.*, vol. 20, no. 3, pp. 226–239, Mar. 1998.

[21] G. Briem, J. A. Benediktsson, and J. R. Sveinsson, "Multiple classifiers applied to multisource remote sensing data," *IEEE Trans. Geosci. Remote Sens.*, vol. 40, no. 10, pp. 2291–2299, Oct. 2002.

[22] G. Fumera and F. Roli, "A theoretical and experimental analysis of linear combiners for multiple classifier systems," *IEEE Trans. Pattern Anal. Mach. Intell.*, vol. 27, no. 6, pp. 942–956, Jun. 2005.

[23] Y.-C. Tzeng, "Remote sensing images classification/data fusion using distance weighted multiple classifiers systems," in *Proc. PDCAT*, Taipei, Taiwan, Dec. 2006.

[24] S. Beucher and C. Lantuejoul, "Use of watersheds in contour detection," in *Proc. Int. Workshop Image Process. Real-Time Edge Motion Detection/Estimation*, Rennes, France, Sep. 1979.

[25] G. Noyel, J. Angulo, and D. Jeulin, "Morphological segmentation of hyperspectral images," *Image Anal. Stereol.*, vol. 26, pp. 101–109, 2007.

[26] A. Evans and X. Liu, "A morphological gradient approach to color edge detection," *IEEE Trans. Image Process.*, vol. 15, no. 6, pp. 1454–1463, Jun. 2006.

[27] L. Vincent and P. Soille, "Watersheds in digital spaces: An efficient algorithm based on immersion simulations," *IEEE Trans. Pattern Anal. Mach. Intell.*, vol. 13, no. 6, pp. 583–598, Jun. 1991.

[28] J. Astola, P. Haavisto, and Y. Neuvo, "Vector median filters," *Proc. IEEE*, vol. 78, no. 4, pp. 678–689, Apr. 1990.

[29] P. Masson and W. Pieczynski, "SEM algorithm and unsupervised segmentation of satellite images," *IEEE Trans. Geosci. Remote Sens.*, vol. 31, no. 3, pp. 618–633, May 1993.

[30] L. Shapiro and G. Stockman, *Computer Vision*. Englewood Cliffs, NJ: Prentice-Hall, 2002.

[31] A. Jensen and A. Solberg, "Fast hyperspectral feature reduction using piecewise constant function approximations," *IEEE Geosci. Remote Sens. Lett.*, vol. 4, no. 4, pp. 547–551, Oct. 2007.

[32] J. C. Tilton, HSEG/RHSEG, HSEGViewer and HSEGReader User's Manual (Version 1.40), 2008, Provided With the Evaluation Version of RHSEG. [Online]. Available: http://techtransfer.gsfc.nasa.gov/ft_tech_rhseg.shtm

[33] J. Tilton, "Analysis of hierarchically related image segmentations," in *Proc. IEEE Workshop Adv. Tech. Anal. Remotely Sensed Data*, 2003, pp. 60–69.

[34] Y. Tarabalka, J. Chanussot, and J. A. Benediktsson, "Spectral–spatial classification of hyperspectral images using segmentation-derived adaptive neighborhoods," in *Multivariate Image Processing*. New York: Wiley, 2009, pp. 341–374.

[35] A. J. Plaza and J. C. Tilton, "Automated selection of results in hierarchical segmentations of remotely sensed hyperspectral images," in *Proc. IGARSS*, Jul. 2005, vol. 7, pp. 4946–4949.

[36] G. Licciardi, F. Pacifici, D. Tuia, S. Prasad, T. West, F. Giacco, J. Inglada, E. Christophe, J. Chanussot, and P. Gamba, "Decision fusion for the classification of hyperspectral data: Outcome of the 2008 GRS-S data fusion contest," *IEEE Trans. Geosci. Remote Sens.*, vol. 47, no. 11, pp. 3857–3865, Nov. 2009.

[37] V. Vapnik, *Statistical Learning Theory*. New York: Wiley, 1998.

[38] J. Stawiaski, "Mathematical morphology and graphs: Application to interactive medical image segmentation," Ph.D. dissertation, Paris School Mines, Paris, France, 2008.

[39] R. C. Prim, "Shortest connection networks and some generalizations," *Bell Syst. Technol. J.*, vol. 36, no. 6, pp. 1389–1401, Nov. 1957.

[40] T. H. Cormen, C. E. Leiserson, R. L. Rivest, and C. Stein, *Introduction to Algorithms,* 2nd ed. Cambridge, MA: MIT Press, 2001.

[41] J. A. Richards and X. Jia, *Remote Sensing Digital Image Analysis: An Introduction*. New York: Springer-Verlag, 1999.

[42] G. M. Foody, "Thematic map comparison: Evaluating the statistical significance of differences in classification accuracy," *Photogramm. Eng. Remote Sens.*, vol. 70, no. 5, pp. 627–633, 2004.

[43] N. Cristianini and J. Shawe-Taylor, *Support Vector Machines and Other Kernel-Based Learning Methods*. Cambridge, U.K.: Cambridge Univ. Press, 2000.

[44] N. Keshava, "A survey of spectral unmixing algorithms," *Lincoln Lab. J.*, vol. 14, no. 1, pp. 55–78, Jan. 2003.

[45] C. Rouquet and P. Bonton, "Region-based segmentation of textured images," in *Proc. ICIAP*, London, U.K., 1995, pp. 11–16.

Yuliya Tarabalka (S'08) received the B.S. degree in computer science from Ternopil Ivan Pul'uj State Technical University, Ternopil, Ukraine, in 2005, the M.Sc. degree in signal and image processing from the Grenoble Institute of Technology (INPG), Grenoble, France, in 2007, the Ph.D. degree in signal and image processing from INPG, and the Ph.D. degree in electrical engineering from the University of Iceland, Reykjavik, Iceland, in 2010.

From July 2007 to January 2008, she was a Researcher with the Norwegian Defence Research Establishment, Norway. She is currently with the Faculty of Electrical and Computer Engineering, University of Iceland, and also with the Grenoble Images Speech Signals and Automatics Laboratory (GIPSA-Lab), INPG, Saint-Martin-d'Hères, France. Her current research work is funded by the "HYPER-I-NET" Marie Curie Research Training Network. Her research interests are in the areas of image processing, pattern recognition, hyperspectral imaging, and development of efficient algorithms.

Jón Atli Benediktsson (S'84–M'90–SM'99–F'04) received the Cand.Sci. degree in electrical engineering from the University of Iceland, Reykjavik, Iceland, in 1984 and the M.S.E.E. and Ph.D. degrees from Purdue University, West Lafayette, IN, in 1987 and 1990, respectively.

He is currently Pro Rector for Academic Affairs and Professor of electrical and computer engineering with the University of Iceland. His research interests are in remote sensing, pattern recognition, neural networks, image processing, and signal processing, and he has published extensively in those fields.

Dr. Benediktsson is a member of Societas Scinetiarum Islandica and Tau Beta Pi. He was Editor of the IEEE TRANSACTIONS ON GEOSCIENCE AND REMOTE SENSING (TGARS) from 2003 to 2008. He has been on the Administrative Committee of the IEEE Geosicence and Remote Sensing Society (GRSS) from 2000 and is the GRSS Executive Vice President for 2010–2011. He was the recipient of the Stevan J. Kristof Award from Purdue University in 1991 as outstanding graduate student in remote sensing, the Icelandic Research Council's Outstanding Young Researcher Award In 1997, the IEEE Third Millennium Medal in 2000, the yearly research award from the Engineering Research Institute of the University of Iceland in 2006, and the Outstanding Service Award from the GRSS in 2007. He was also a corecipient of the University of Iceland's Technology Innovation Award in 2004.

Jocelyn Chanussot (M'04–SM'04) received the M.Sc. degree in electrical engineering from the Grenoble Institute of Technology (INPG), Grenoble, France, in 1995, and the Ph.D. degree from Savoie University, Annecy, France, in 1998.

In 1999, he was with the Geography Imagery Perception Laboratory for the Delegation Generale de l Armement (DGA-French National Defense Department). Since 1999, he has been with INPG, where he was an Assistant Professor from 1999 to 2005, an Associate Professor from 2005 to 2007, and is currently a Professor of signal and image processing. He is currently conducting his research at the Grenoble Images Speech Signals and Automatics Laboratory (GIPSA-Lab), INPG, Saint-Martin-d'Hères, France. His research interests include image analysis, multicomponent image processing, nonlinear filtering, and data fusion in remote sensing.

Dr. Chanussot is an Associate Editor of the IEEE TRANSACTIONS ON GEOSCIENCE AND REMOTE SENSING. He is the Cochair of the GRS Data Fusion Technical Committee (2005–2008) and a member of the Machine Learning for Signal Processing Technical Committee of the IEEE Signal Processing Society (2006–2008). He is the founding President of IEEE GRS French chapter (2007).

James C. Tilton (S'79–M'81–SM'94) received B.A. degree in electronic engineering, environmental science and engineering, and anthropology, and the M.E.E. degree in electrical engineering from Rice University, Houston, TX, in 1976, the M.S. degree in optical sciences from the University of Arizona, Tucson, in 1978, and the Ph.D. degree in electrical engineering from Purdue University, West Lafayette, IN, in 1981.

He is currently a Computer Engineer with the Computational and Information Sciences and Technology Office (CISTO), Science and Exploration Directorate, NASA Goddard Space Flight Center, Greenbelt, MD. As a member of the CISTO, he is responsible for designing and developing computer software tools for space and Earth science image analysis and encouraging the use of these computer tools through interactions with space and Earth scientists. He is the holder of a patent with two other pending patent applications for his development of a recursive hierarchical segmentation algorithm.

Dr. Tilton is a Senior Member of the IEEE Geoscience and Remote Sensing Society and the IEEE Signal Processing Society and is a member of Phi Beta Kappa, Tau Beta Pi, and Sigma Xi. From 1992 to 1996, he served as a member of the IEEE Geoscience and Remote Sensing Society Administrative Committee. Since 1996, he has served as an Associate Editor of the IEEE TRANSACTIONSON GEOSCIENCE AND REMOTE SENSING.